Electronic structure of $TiSe_2$ from a quasi-self-consistent G_0W_0 approach

Maria Hellgren [1,2] Lucas Baguet [1] Matteo Calandra,[3,4] Francesco Mauri,[5] and Ludger Wirtz [6]

[1]*Sorbonne Université, Muséum National d'Histoire Naturelle, UMR CNRS 7590, Institut de Minéralogie, de Physique des Matériaux et de Cosmochimie (IMPMC), 4 place Jussieu, 75005 Paris, France*

[2]*European Theoretical Spectroscopic Facility (ETSF)*

[3]*Dipartimento di Fisica, University of Trento, Via Sommarive 14, 38123 Povo, Italy*

[4]*Sorbonne Universités, CNRS, Institut des Nanosciences de Paris, UMR7588, 75252 Paris, France*

[5]*Dipartimento di Fisica, Universita di Roma La Sapienza, Piazzale Aldo Moro 5, I-00185 Roma, Italy*

[6]*Department of Physics and Materials Science, University of Luxembourg, 162a avenue de la Faïencerie, L-1511 Luxembourg, Luxembourg*

(Received 29 May 2020; revised 16 January 2021; accepted 19 January 2021; published 1 February 2021)

In a previous work, it was shown that the inclusion of exact exchange is essential for a first-principles description of both the electronic and the vibrational properties of $TiSe_2$, M. Hellgren *et al.* [Phys. Rev. Lett. **119**, 176401 (2017)]. The *GW* approximation provides a parameter-free description of screened exchange but is usually employed perturbatively (G_0W_0), making results more or less dependent on the starting point. In this work, we develop a quasi-self-consistent extension of G_0W_0 based on the random phase approximation (RPA) and the optimized effective potential of hybrid density functional theory. This approach generates an optimal G_0W_0 starting point and a hybrid exchange parameter consistent with the RPA. While self-consistency plays a minor role for systems such as Ar, BN, and ScN, it is shown to be crucial for TiS_2 and $TiSe_2$. We find the high-temperature phase of $TiSe_2$ to be a semimetal with a band structure in good agreement with experiment. Furthermore, the optimized hybrid functional agrees well with our previous estimate and therefore accurately reproduces the low-temperature charge-density-wave phase.

DOI: 10.1103/PhysRevB.103.075101

I. INTRODUCTION

$TiSe_2$ is a layered quasi-two-dimensional material that undergoes an unconventional charge-density-wave (CDW) transition below 200 K. The apparent interplay between the CDW and superconductivity at finite pressure or doping [1,2] has led to numerous studies over the past years aiming to understand the driving mechanism behind the CDW. Nevertheless, the relative role played by excitonic effects and electron-phonon coupling is still debated. Experimentally, strong signatures are observed in both vibrational [3–6] and angle-resolved photoemission spectra (ARPES) [7–13], and some studies point to soft electronic modes [14].

First-principles calculations should be able to explain the exact mechanism of the CDW transition. However, numerically tractable approaches such as the local density approximation (LDA) or generalized gradient approximations (GGAs) within density functional theory (DFT) fail to give a complete picture [5,15,16]. A dramatic improvement is found when including a fraction of Hartree-Fock (HF) exchange via the hybrid functionals [12,17,18]. With a result similar to the DFT + U approach [16,19], the Ti-d levels are then well described. In addition, the hybrid functionals contain the long-range Coulomb interaction, which was shown to be crucial to induce the CDW phase [18]. This fact suggests that strong electron-hole coupling is at play and that an excitonic transition could be of importance [20,21]. On the other hand, it was also found that the standard medium-range hybrid functional already gives a quantitatively reasonable agreement between theory and experiment. However, the results were also shown to be strongly dependent on the hybrid parameters, making it still uncertain whether a parametrization optimized on a test-set of standard semiconductors is adequate.

The *GW* method is computationally more expensive but provides a parameter-free and physical description of screened exchange. The bare Coulomb interaction is replaced by the screened Coulomb interaction, W, which is determined by the linear density response function approximated at the Hartree level, i.e., the random phase approximation (RPA) [22,23]. The *GW* approximation for the self-energy is known to produce accurate band gaps on a wide range of systems [24–27]. It is, however, almost always employed perturbatively (G_0W_0), on top of a DFT Kohn-Sham (KS) band structure, assuming that the KS electronic structure is close enough to the final result. Other variants that bring results closer to self-consistency have also been developed [28–31]. An alternative to the fully self-consistent *GW* scheme is to look for the optimal KS starting-point via the Sham-Schlüter equation [32–34]. The resulting KS potential produces a density similar to the *GW* density and is known as the RPA potential [35,36]. The KS RPA band structure can be shown to provide a consistent starting-point for G_0W_0 [37,38].

A high-level calculation of the electronic band structure of $TiSe_2$ in the high-T phase would be valuable. While transport experiments all predict a semimetallic behavior, some ARPES measurements have found a gap [7,8]. The latter scenario was supported by the first G_0W_0 calculation and interpreted as an excitonic gap [39]. In this work, we will

reexamine how G_0W_0 performs on $TiSe_2$ by first showing that it is a case sensitive to exchange in the starting-point. As a fully self-consistent calculation is out of reach, we develop a quasi-self-consistent approach that exploits the local hybrid potential as an approximation to the local RPA potential. In this way, we produce a theoretically justified G_0W_0 solution that approximates the RPA solution. At the same time, we generate an RPA-optimized hybrid functional that is used to study the CDW phase.

The paper is organized as follows. In Sec. II we start by reviewing the *GW* formalism and the RPA as a self-consistent way to do perturbative G_0W_0. We then introduce a hybrid functional approach based on the optimized effective potential. Using this potential, we then develop a quasi-self-consistent G_0W_0 scheme and compare it to variants introduced by others. In Sec. III we present numerical results for Ar, BN, ScN, TiS_2, and $TiSe_2$. We also use the RPA optimized hybrid functional to study the CDW phase of $TiSe_2$. Finally, in Sec. IV we present our conclusions.

II. SCREENED EXCHANGE FROM *GW*

We will focus on studying the performance of the *GW* approximation in describing the band structure of the high-T phase of $TiSe_2$. The results turn out to be strongly dependent on which approximate *GW* scheme is used. In this section, therefore, we start by reviewing the different ways to solve the *GW* equations, and we discuss the connections between *GW*, RPA, COHSEX (COulomb Hole Screened EXchange), and hybrid functionals. This will allow us to finally motivate a quasi-self-consistent G_0W_0 approach based on the local hybrid potential.

A. The *GW* approximation

We define the self-energy as the nonlocal frequency-dependent potential Σ that contains all the many-body effect beyond the Hartree (H) approximation. To first order, in an expansion in terms of the Green's function, G, and the Coulomb interaction, v, Σ is just the static but nonlocal Fock term of the HF approximation,

$$\Sigma^{\mathrm{HF}} = iGv. \tag{1}$$

By replacing the bare Coulomb interaction in the Fock term with the dynamically screened Coulomb interaction, W, we obtain the self-energy within the *GW* approximation,

$$\Sigma = iGW. \tag{2}$$

The screened interaction within the *GW* approximation is approximated at the time-dependent Hartree level for which the irreducible polarizability, P, is approximated with P_0, i.e., to zeroth order in the explicit dependence on the Coulomb interaction. We thus have

$$W = v + vP_0W, \quad P_0 = -iGG. \tag{3}$$

From Dyson's equation,

$$G = G_{\mathrm{H}} + G_{\mathrm{H}}\Sigma[G]G, \tag{4}$$

we then have access to the many-body quasiparticle spectrum contained in G.

It can further be shown that the *GW* approximation is a Φ-derivable approximation [40,41] that obeys physical conservation laws and has an underlying action functional. An example of such an action functional is the Klein functional [42]

$$Y_{\mathrm{K}} = -i\Phi[G] - U_{\mathrm{H}} + i\mathrm{Tr}\left[GG_{\mathrm{H}}^{-1} - 1 + \ln(-G^{-1})\right], \tag{5}$$

where U_{H} is the Hartree energy. With the choice

$$\Phi[G] = \tfrac{1}{2}\mathrm{Tr}\{\ln[1 + ivGG]\} \tag{6}$$

it is easy to see that Y_{K} is stationary when G obeys Dyson's equation [Eq. (4)], and the self-energy is equal to

$$\Sigma = \frac{\delta\Phi}{\delta G} = iGW. \tag{7}$$

At the stationary point, the Klein functional is equal to the *GW* total energy as obtained from the standard nonvariational Galitskii-Migdal energy expression.

Instead of using the Hartree approximation as the zeroth-order approximation for G, one can start from the DFT KS system. Dyson's equation can then be rewritten in terms of the single-particle KS Green's function, G_s, and the exchange-correlation (xc) part of the local KS potential,

$$G = G_s + G_s[\Sigma[G] - v_{\mathrm{xc}}]G. \tag{8}$$

The diagonal of G, i.e., the density, is already exactly described by G_s. In this way, G_s can be assumed to be "close" to G, justifying a perturbative treatment of Eq. (8), and thus circumventing the full solution to the numerically challenging Dyson's equation. By writing Eq. (8) in the basis of KS orbitals and keeping only the diagonal terms, we can write the quasiparticle equation as [25,43]

$$E_k = \varepsilon_k + \langle k|\Sigma_s(E_k) - v_{\mathrm{xc}}|k\rangle, \tag{9}$$

where k refers to the Bloch orbital index. The subscript s on the self-energy signifies that it is evaluated with G_s. The energy dependence of Σ_s can either be treated to zeroth order, i.e., $E_k = \varepsilon_k$, where ε_k is the KS eigenvalue, or to first order in a Taylor expansion around ε_k. The latter implies that a renormalization factor

$$Z_k = \left[1 - \frac{\partial\,\mathrm{Re}\Sigma_s}{\partial\omega}\bigg|_{\omega=\varepsilon_k}\right]^{-1} \tag{10}$$

should be multiplied in the following way:

$$E_k = \varepsilon_k + Z_k\langle k|\Sigma_s(\varepsilon_k) - v_{\mathrm{xc}}|k\rangle. \tag{11}$$

This G_0W_0 correction, starting from PBE or LDA, is the most common *GW* approach to determine the band structure. The justification of this approach relies, however, on the assumption that PBE or LDA orbitals are similar to the true quasiparticle orbitals. The renormalization factors are usually incorporated, but it can be argued that these should be omitted [37]. The arguments are based on the connection between *GW* and the RPA for the total energy [35,44,45], as we will now discuss.

Let us go back to the Klein energy functional [Eq. (5)] and keep the Φ-functional in the *GW* approximation. From now on we will add superscripts (Φ^{GW}, Σ^{GW}) as we focus only on this approximation. If we replace the interacting G, in every term,

with a noninteracting G_s, we can, after a few manipulations, write Eq. (5) as

$$Y_K^{GW}[G_s] = -i\Phi^{GW}[G_s] + T_s[n] + U_{\rm H} + U_{\rm ext}, \tag{12}$$

where T_s is the kinetic energy of noninteracting KS electrons, and $U_{\rm ext}$ is the external potential energy. It is easy to see that $\Phi^{GW}[G_s]$ is exactly the same functional as the xc energy of the RPA energy functional,

$$E_{\rm xc}^{\rm RPA} \equiv -i\Phi^{GW}[G_s] = -\frac{i}{2}{\rm Tr}\{\ln[1 + iv G_s G_s]\}. \tag{13}$$

Equation (12) is thus merely the RPA total energy, i.e., $Y_K^{GW}[G_s] = E^{\rm RPA}$ [35,45,46].

The RPA energy functional can be shown to have a minimum when varied with respect to the total KS potential $V_s = v_{\rm ext} + v_{\rm H} + v_{\rm xc}$. Such a variation can be carried out via the functional $G_s[V_s]$. At the minimum $v_{\rm xc} = v_{\rm xc}^{\rm RPA}$ obeys the so-called linearized Sham-Schlüter (LSS) equation

$$\int d2\, \chi_s(1,2) v_{\rm xc}^{\rm RPA}(2) = \int d2\, d3\, \Lambda_s(3,2;1)\Sigma_s^{GW}(2,3), \tag{14}$$

where $\Lambda_s(3,2;1) = -iG_s(3,1)G_s(1,2)$ and $\chi_s(2,1) = -iG_s(2,1)G_s(1,2)$ [47]. The LSS equation can also be derived from the condition that the GW density and the KS RPA density, i.e., the diagonals of G and G_s, are the same to first order when expanding Dyson's equation [Eq. (8)].

As the RPA potential is a local KS potential, it does not reproduce the fundamental gap [32–34]. One can, however, still calculate the gap, E_g, corresponding to the RPA functional by taking the derivative of the energy functional with respect to particle number N. One finds

$$E_g = I - A = \left.\frac{\partial E^{\rm RPA}}{\partial N}\right|_+ - \left.\frac{\partial E^{\rm RPA}}{\partial N}\right|_-. \tag{15}$$

Evaluating the derivative on the right-hand side "+," i.e., the negative of the ionization energy

$$-I = \varepsilon_v + \langle v|\Sigma_s^{GW}(\varepsilon_v) - v_{\rm xc}^{\rm RPA}|v\rangle \tag{16}$$

and the derivative on the left hand side "−," i.e., the negative of the affinity

$$-A = \varepsilon_c + \langle c|\Sigma_s^{GW}(\varepsilon_c) - v_{\rm xc}^{\rm RPA}|c\rangle, \tag{17}$$

we can write

$$E_g = E_g^{\rm KS} + \Delta_{\rm xc}, \tag{18}$$

where $E_g^{\rm KS}$ is the KS gap and

$$\Delta_{\rm xc} = \langle c|\Sigma_s^{GW}(\varepsilon_c) - v_{\rm xc}^{\rm RPA}|c\rangle - \langle v|\Sigma_s^{GW}(\varepsilon_v) - v_{\rm xc}^{\rm RPA}|v\rangle. \tag{19}$$

To derive these expressions, Eq. (14) has to be used. The quantity $\Delta_{\rm xc}$ equals what is called the derivative discontinuity within DFT [48–51].

It is now clear that the gap obtained from the RPA functional is merely the G_0W_0 correction of Eq. (11), without the Z_k factor, evaluated with the RPA potential. The RPA potential can thus be seen as an optimal KS starting point for G_0W_0, which produces a gap equal to the gap extracted from the RPA functional [37]. It has been shown on a number of semiconductors [38] that using the RPA potential for a G_0W_0 calculation brings gaps in closer agreement with self-consistent GW approaches [30].

By expanding the GW quasiparticle energy around the zeroth-order RPA KS energy and using Eq. (14), the expressions in Eqs. (16) and (17) are easily extended to the whole band structure [37],

$$E_k^{\rm RPA} = \varepsilon_k + \langle k|\Sigma_s^{GW}(\varepsilon_k) - v_{\rm xc}^{\rm RPA}|k\rangle. \tag{20}$$

To conclude, we have reviewed how it is possible to calculate gaps and even the full band structure from the RPA, and that this corresponds to the perturbative G_0W_0 result evaluated with the local RPA potential. These are well-known results upon which we will base the following discussions.

B. Hybrid functionals and the COHSEX approximation

We will now turn to the simpler COHSEX and hybrid functionals, which are often used as cheaper but self-consistent alternatives to the GW approach.

The frequency dependence of the GW self-energy allows for the description of many-body effects such as quasiparticle lifetimes and satellite spectra but severely complicates a fully self-consistent solution. Often one is, however, only interested in the quasiparticle excitation energy for which the nonlocality of the self-energy plays the most important role. One is then motivated to approximate Σ by ignoring the dynamical effects in W. This implies setting

$$W_{\rm static} = v + vP_0(\omega = 0)W_{\rm static}, \tag{21}$$

and results in the so-called COHSEX approximation

$$\Sigma^{\rm COHSEX} = iGW_{\rm static} + \tfrac{1}{2}W_p^d, \tag{22}$$

where $W_p^d = {\rm diag}[vP_0(\omega = 0)W_{\rm static}]$ is a local Coulomb-hole potential, and the first term is a nonlocal statically screened exchange operator. The COHSEX approximation can easily be solved self-consistently but can still be numerically demanding since it requires the generation and summation over all conduction bands. A more drastic approach that avoids the inclusion of unoccupied bands is to keep the bare Coulomb interaction as in the HF approximation but scale it down with a constant α. If we then add a compensating fraction of the local PBE exchange and a local PBE correlation term, we get the so-called hybrid functionals

$$\Sigma^{{\rm HYB},\alpha} = \alpha\Sigma^{\rm HF} + (1-\alpha)v_{\rm x}^{\rm PBE} + v_{\rm c}^{\rm PBE}. \tag{23}$$

These functionals are structurally similar to COHSEX but not more demanding than a HF calculation. One of the drawbacks is that a free parameter is introduced. A fraction 25% (PBE0) has shown to be reasonable in many molecular systems. In the HSE06 functional, a second parameter, $\mu = 0.2\,\text{Å}^{-1}$, that controls the range of the Coulomb interaction is introduced [52]. In this way, it is possible to get a good description of many semiconductors as well.

Although often used in a DFT context, the hybrid functionals are almost always treated like the HF approximation, that is, by minimizing the energy with respect to orbitals that are generated by the nonlocal Fock potential. In this work, we will instead use the optimized effective potential method [53] and minimize the hybrid energy with respect to a local KS potential. The local KS potential corresponding to HF has

been evaluated for solids before and is know as the exact-exchange (EXX) potential [54,55]. The local hybrid potential is given by the sum of the local potentials derived from the PBE terms and a local exchange potential obtained from an equation similar to the LSS equation [Eq. (14)] but with Σ_s^{GW} replaced by the scaled HF self-energy. We have

$$v_{\rm xc}^{{\rm hyb},\alpha} = v_{\rm x}^{\alpha} + (1-\alpha)v_{\rm x}^{\rm PBE} + v_{\rm c}^{\rm PBE}, \tag{24}$$

where

$$\int d2\,\chi_s(1,2)v_{\rm x}^{\alpha}(2) = \alpha \int d2\,d3\,\Lambda_s(3,2;1)\Sigma_s^{\rm HF}(2,3). \tag{25}$$

The potential $v_{\rm x}^{\alpha}$ can again be seen as the local potential giving a density similar to the density of the fully nonlocal potential, to first order. The gap will, however, differ from the gap of the nonlocal potential, but, when corrected with the discontinuity

$$\Delta_{\rm xc} = \langle c|\alpha\Sigma_s^{\rm HF} - v_{\rm x}^{\alpha}|c\rangle - \langle v|\alpha\Sigma_s^{\rm HF} - v_{\rm x}^{\alpha}|v\rangle, \tag{26}$$

the gap is expected to be close to that of the nonlocal hybrid functional. Gaps calculated in this way using other exchange-based functionals can be found in Refs. [56,57].

C. Optimal G_0W_0 starting-point based on a local hybrid potential

The common crucial ingredient in *GW*, COHSEX, and hybrid functionals is the nonlocal exchange term. Due to this similarity, the hybrids can be used as a way to do approximate self-consistent *GW*. Such an approach was developed in Refs. [31,58]. By using a hybrid as a starting-point for G_0W_0, the α parameter is varied until the *GW* correction vanishes. At this value, the *GW* and hybrid eigenvalues agree,

$$\langle k|\Sigma_s^{GW}\left(\varepsilon_k^{\rm nl}\right) - \Sigma_s^{{\rm HYB},\alpha}|k\rangle_{\rm nl} = 0 \Rightarrow E_k^{GW} = \varepsilon_k^{\rm nl}. \tag{27}$$

Here the matrix elements are evaluated with orbitals generated by the nonlocal $\Sigma_s^{{\rm HYB},\alpha}$, emphasized by the subscript (superscript) "nl." This method has been shown to perform well for molecules, improving the ionization energies as compared to standard hybrid functionals and G_0W_0 based on the PBE starting-point [31]. We note, however, that it is not possible to derive an equation similar to Eq. (18) combining the Klein *GW* energy functional with a nonlocal potential. In fact, it has been shown to lack an extremum when varied in a restricted space of nonlocal but static potentials [59].

We will now present a variant that utilizes the RPA energy and, hence, the optimization with respect to a *local* potential. As seen in the previous subsection, a G_0W_0 correction based on the local RPA potential is justified via the *GW* LSS equation [Eqs. (14) and (20)]. Analogously, a hybrid correction based on the local hybrid potential is justified via the hybrid LSS equation. We have

$$E_k^{{\rm HYB},\alpha} = \varepsilon_k + \langle k|\Sigma_s^{{\rm HYB},\alpha} - v_{\rm xc}^{{\rm hyb},\alpha}|k\rangle. \tag{28}$$

We will now approximate the RPA potential in Eq. (20) by the local hybrid potential

$$E_k^{\rm RPA} \approx \varepsilon_k + \langle k|\Sigma_s^{GW}(\varepsilon_k) - v_{\rm xc}^{{\rm hyb},\alpha}|k\rangle \tag{29}$$

and optimize α such that the corrections in Eqs. (28) and (29) are equal. This is equivalent to

$$\langle k|\Sigma_s^{GW}(\varepsilon_k) - \Sigma_s^{{\rm HYB},\alpha}|k\rangle = 0 \Rightarrow E_k^{\rm RPA} = E_k^{{\rm HYB},\alpha}, \tag{30}$$

where the self-energy operators are evaluated with orbitals and eigenvalues from $v_{\rm xc}^{{\rm hyb},\alpha}$ [instead of $\Sigma_s^{{\rm HYB},\alpha}$ as in Eq. (27) above]. In this way, we optimize α such that the DFT hybrid functional behaves like the RPA functional when varying the particle number. The difference between this approach and the one in Ref. [31] lies in which type of reference system is used to evaluate the *GW* energy. Allowing for nonlocal potentials can have a large impact on the energy due to the opening of a large gap.

Due to a lack of frequency dependence in $\Sigma_s^{{\rm HYB},\alpha}$, the condition in Eq. (30) is, in general, impossible to fulfill for all bands at every k, but it can be made true for the difference between the highest occupied level and the lowest unoccupied level. One thus needs to optimize α using the following condition:

$$\langle c|\Sigma_s^{GW}(\varepsilon_c) - \Sigma_s^{{\rm HYB},\alpha}|c\rangle - \langle v|\Sigma_s^{GW}(\varepsilon_v) - \Sigma_s^{{\rm HYB},\alpha}|v\rangle = 0. \tag{31}$$

Let us now compare this approach to other *GW*-schemes. The most common way to include some form of self-consistency within *GW* is to iterate the eigenvalues, i.e., solving Eq. (9), while keeping the KS orbitals fixed at the PBE level. This works well under the assumption that xc effects beyond PBE are unimportant for the orbitals. An advantage of our approach is that it does not rely on this assumption as it takes into account both eigenvalues and orbitals at the same level of approximation. Another, more advanced, approach, which takes into account changes in the orbitals via a static but nonlocal potential, is the "quasiparticle self-consistent *GW*" of Ref. [29]. This approach requires, however, the generation of the full self-energy matrix and not just the diagonal terms, making it more expensive than the approach suggested here. Results from this approach have shown that, indeed, self-consistency in the orbitals is important [65].

In the next section, we will show that self-consistency has a very small effect on systems where PBE already gives a good description of the orbitals. In contrast, for systems where exact-exchange plays an important role, self-consistency is necessary and we will show that, via Eq. (31), it is possible to obtain meaningful results. The validity of the G_0W_0-approach is determined by the validity of the RPA for the given system. Furthermore, by approximating the RPA potential with the local hybrid potential, we generate, as a by-product, a hybrid functional that can be used to study other properties such as phonons and lattice instabilities.

III. NUMERICAL RESULTS

In this section, we start by introducing $TiSe_2$ and the technical aspects of our calculations. We then present the G_0W_0 results for $TiSe_2$, TiS_2, and a set of well-known systems (Ar, c-BN, and ScN) for which there already exist both EXX and G_0W_0 results in the literature. Finally, we investigate the performance of the RPA optimized hybrid functional in capturing the CDW phase of $TiSe_2$.

A. System and computational details

The high-T phase of $TiSe_2$ crystallizes in the space group $P\bar{3}m1$. It belongs to the $1T$ family of the layered

TABLE I. Band gaps (eV) of Ar, *c*-BN, ScN, TiS_2, and $TiSe_2$. The G_0W_0 results (without renormalization factor) are obtained with G_0 of the approximation in the preceding column. The H-G_0W_0 results are evaluated with the optimized nonlocal hybrid functional having an equal gap. The EXX results for Ar, BN, and ScN are compared to EXX results found in the literature. EXX_c corresponds to EXX plus a correlation term at the PBE level. All results (EXX, EXX_c, and lhyb) for TiS_2 and $TiSe_2$ are obtained with $\mu = 0.1$ Å^{-1}.

Solid	PBE	G_0W_0	EXX	EXX lit.	EXX_c	G_0W_0	α	lhyb	G_0W_0	α	H-G_0W_0	HSE06	Expt.
Ar	8.65	14.09	9.57	9.61[a]	9.93	14.30	0.57	9.38	14.19	0.63	14.88	10.32	14.2[b]
BN	4.54	6.51	5.58	5.57[c]	5.12	6.78	0.25	4.70	6.61	0.30	6.99	5.85	6.4 ± 0.5[c]
ScN	−0.05	1.01	1.57	1.58[d]	1.39	0.81	0.17	0.21	0.96	0.24	1.51	0.92	0.9 ± 0.1[e]
TiS_2	−0.10	1.18	1.18		1.03	0.30	0.25	0.17	0.82	0.33	1.17	0.57	0.5 ± 0.1[f]
$TiSe_2$	−0.63	0.37	0.57		0.38	−0.85	0.20	−0.45	−0.07	0.32	0.40	−0.15	−0.1–0.1[g]

[a]Reference [38].
[b]Reference [60].
[c]Reference [61].
[d]Reference [62].
[e]Reference [63].
[f]Reference [64].
[g]See the text.

transition-metal dichalcogenides with the Ti atom octahedrally coordinated by six neighboring Se atoms. A semimetallic behavior is found in most experiments. Below 200 K, a CDW transition occurs, characterized by a $2 \times 2 \times 2$ superstructure (space group $P3\bar{c}1$) and the opening of a small gap. The distortion pattern can be uniquely defined by the displacement δTi and the ratio $\delta\text{Ti}/\delta\text{Se} \approx 3$. Standard DFT functionals predict a phonon instability at the three equivalent *L* points. A symmetric combination of these gives the correct CDW pattern, but with a severely underestimated distortion amplitude [16]. Hybrid functionals give a better description and have revealed the important role of HF exchange for the instability. This possibly hints at the presence of an excitonic instability. Although a weakly screened electron-hole interaction is clearly important, no spontaneous electronic CDW has so far been generated in bulk $TiSe_2$. Hybrid functionals induce the CDW via a strong electron-phonon coupling combined with the enhanced electronic susceptibility at the *L* points. This mechanism is given support by the combined accuracy of the electronic bands, phonons, and distortion amplitude [18].

In this work, we aim for the more sophisticated *GW* method that allows for a physical description of the screened interaction. Due to the increase in computational cost, we have been limited to the high-*T* phase. The low-*T* CDW phase will be studied with the RPA-based hybrid functional, optimized according to the procedure described in the previous section.

In addition, we have determined the gap of TiS_2, which is structurally identical to $TiSe_2$ but lacks a CDW transition, at least in the bulk. We have only found one *GW* study of TiS_2 where the gap was determined to 0.75 eV [66], which can be compared to the experimental result of around 0.5 eV [64]. We have also looked at solid Ar (a van der Waals bonded large-gap insulator), c-BN (an *sp* bonded insulator), and ScN (a *pd* bonded semiconductor) in order to illustrate the workings and validity of the equations derived in Sec. II.

The hybrid calculations have been performed with VASP [67–69], QUANTUM ESPRESSO [70] (QE), and the CRYSTAL program [71]. Whenever comparisons could be made, these codes, despite using different pseudopotentials, or in the latter case a Gaussian basis set, agree rather well. For example, *pd* gaps agree within 0.05 eV. For TiS_2 and $TiSe_2$ we have used a range-separation parameter of $\mu = 0.1$ Å^{-1} in all hybrid calculations. We chose a range twice as large as in HSE06 since our previous work on $TiSe_2$ indicated that HSE06 was somewhat too short-ranged [18]. The local hybrid potential was calculated with QE using an iterative algorithm for solving the LSS integral equation [Eq. (25)] (see Ref. [72] for further details). The *GW* self-energy was subsequently evaluated using the YAMBO code with full frequency integration [73,74]. For testing the optimization scheme in Eq. (27) we switched to the VASP code, which allows the self-energy to be evaluated with a hybrid G_0. Agreement between different codes that use different numerical techniques and pseudopotentials is still hard to achieve within *GW* [75,76]. Nevertheless, for Ar and c-BN, results on the PBE-G_0W_0 level agree within 0.05 eV. For the *pd* gapped systems, we found variations up to 0.1 eV (TiS_2 and $TiSe_2$) and 0.2 eV (ScN), which should be taken into account when comparing the different schemes. We used a $12 \times 12 \times 6$ and $10 \times 10 \times 4$ *k*-point grid for $TiSe_2$ and TiS_2, respectively. Up to 500 unoccupied bands were included in the self-energy.

B. G_0W_0 results

In Table I we present the band gaps of Ar, c-BN, ScN, TiS_2, and $TiSe_2$. The PBE results are presented in the first column, and the G_0W_0 results, obtained on top of the PBE orbitals, are presented in the second column. The renormalization factor is omitted in all G_0W_0 calculations. To demonstrate the accuracy of our implementation of the LSS equation, the gaps obtained within the EXX approximation (third column) are first compared to values found in the literature. We find a very good agreement in all cases where results are available. The EXX_c results are obtained by adding the PBE correlation potential to the EXX potential. This EXX_c potential is then used for obtaining the G_0W_0 results in the next column. In this way, we provide both extremes of the α-range: PBE ($\alpha = 0$) and EXX_c ($\alpha = 1.0$). The α parameter is then optimized according to Eq. (31). The optimized value of α, the KS gap of the corresponding local hybrid potential (lhyb), and the final G_0W_0 gap are presented in the following three columns. As a result

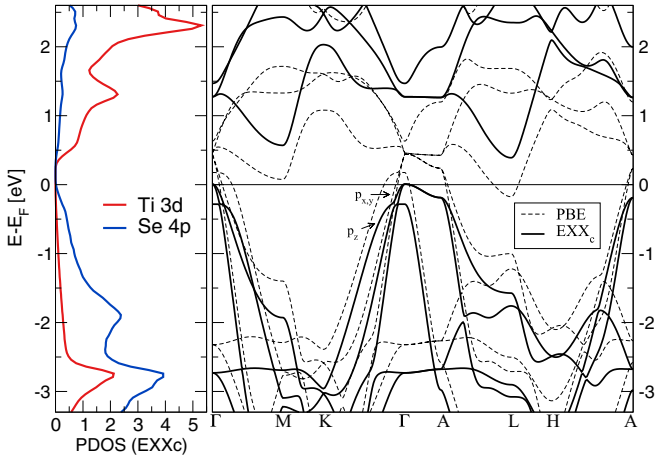

FIG. 1. Band structure and p, d-orbital projected density of states in the high-T phase of $TiSe_2$. EXX_c (full lines) compared to PBE (dashed lines).

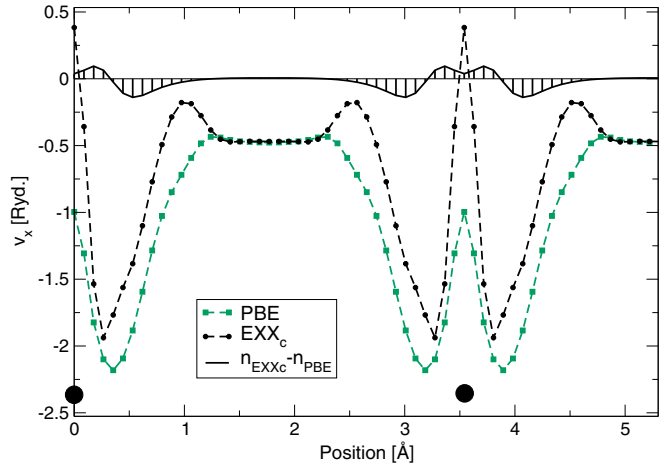

FIG. 2. Exchange part, v_x, of the KS potential along the [100] direction. PBE in green with squares and EXX_c in black with circles. The density difference generated by these potentials is also illustrated (with arbitrary units on the y-axis). Black dots correspond to the position of the Ti atoms.

of Eq. (31), the G_0W_0 gap has to be the same as the perturbative gap of the nonlocal hybrid functional [Eq. (28)] with parameter α. Finally, we present the H-G_0W_0 results, which are obtained using the optimization scheme of Eqs. (27), the HSE06 results, and experimental values.

Looking at the results for Ar and c-BN, we immediately see that the G_0W_0 results are not so sensitive to which KS potential is used. The EXX potential increases the KS gap by around 1 eV, but this leads only to a small increase of 0.2–0.3 eV in the G_0W_0 gap. By optimizing α, we find a gap in between ($\alpha = 0.57$ for Ar and $\alpha = 0.25$ for c-BN). These values are consistent with RPA in a sense that both RPA and the hybrid functional give the same gap when evaluated with the orbitals of the optimized local hybrid potential. We note that the H-G_0W_0 results generally lead to larger values of α.

In ScN, a *pd* semiconductor, we see a partially different behavior. First, PBE predicts a semimetallic ground state with a *pd* band overlap. Including exact-exchange, a KS gap of 1.57 eV opens. This rather large variation produces again only a small variation at the G_0W_0 level. However, the behavior of the correction is opposite as compared to the correction in Ar and c-BN by giving a smaller G_0W_0 gap with EXX_c than with PBE. This somewhat counterintuitive behavior was noted already in Ref. [78]. We now look at TiS_2, which also has a *pd* gap. We see a similar trend but now the *GW* variation is larger, ranging from 0.3 eV with EXX_c to 1.18 eV with PBE. In this case, the optimization plays a crucial role. With 25% of exchange, the gap optimizes to 0.82 eV. After this study, we are now ready to turn to $TiSe_2$.

The high-T phase PBE band structure has been published in several previous works, but is repeated here in Fig. 1. The PBE (and LDA) results differ strongly from ARPES experiments as analyzed in detail in Ref. [16]. Similar to ScN and TiS_2, the Se-p–Ti-d band overlap is severely overestimated and, in this case, even inverted at Γ, leading to strong *pd* hybridization [16]. Furthermore, the p_z orbitals corresponding to the flattened p-band around Γ are pushed above the Fermi level leading to excess d-electron occupation. These large errors invalidate the use of a standard PBE starting-point for G_0W_0. If we use PBE as a starting-point for G_0W_0, we open a gap of 0.37 eV between Γ and L (see Table I). The band gap is actually a bit smaller since we also found "Mexican hat" features around Γ similar to those reported in Ref. [39]. These features were found already in the HF term, but they disappear as soon as the orbitals are updated [18].

In Fig. 1, we also compare the KS band structure of the EXX_c approximation to PBE. The corresponding projected density of states (PDOS) is shown in the side panel. The inclusion of exchange, even with a KS local potential, corrects the occupations and opens a gap between Γ and L. Including the discontinuity [Eq. (26)], the gap becomes as large as 3.75 eV, in agreement with a HF_c calculation.

In Fig. 2 we have plotted the exchange part of the corresponding KS potentials (PBE and EXX_c). The accuracy of our LSS implementation can be seen from the smoothness of our EXX_c potential. In EXX_c we see additional structures around the Ti atom that are missing in PBE. These barrierlike features typically act to localize charges. Looking at the density difference, EXX_c contracts the density around the Ti atom. According to Eq. (25), we expect a similar behavior in the HF_c approximation.

If we evaluate G_0W_0 on top of the EXX_c band structure, the gap closes and we find a large band overlap (−0.85 eV). The magnitude of the variation is very close to the one in TiS_2, and it is clear that a self-consistent scheme is necessary. At optimal $\alpha = 0.2$, we find a small band overlap of around 0.1 eV. ARPES has predicted results between −0.1 and 0.1 eV in the high-T phase [7–13]. Our value is thus a reasonable prediction and shows that even a metallic solution can be found within *GW*. The electron-phonon mechanism found in Ref. [18] did not crucially depend on the existence of a Fermi surface, but a semimetallic solution increases the probability for the existence of a purely electronic CDW.

The band structure along Γ-M and A-L is shown in Fig. 3 superimposed on the full band structure of a hybrid functional with 20% of exchange ($HYB^{\alpha=0.2}$). We see that not only does

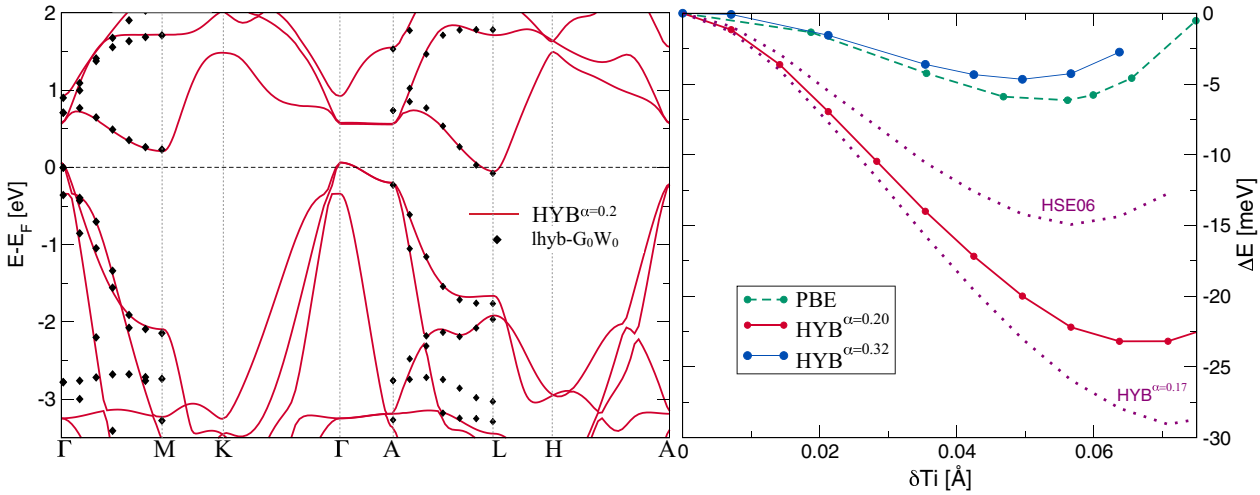

FIG. 3. Left: band structure of the optimal hybrid functional with 20% of nonlocal exchange ($HYB^{\alpha=0.2}$) compared to the corresponding lhyb-G_0W_0 result. Right: energy gain in the supercell as a function of Ti-distortion keeping the ratio $\delta\mathrm{Ti}/\delta\mathrm{Se} = 3$ fixed. Optimal hybrid (red) is shown together with PBE (green) and the hybrid functional of the H-G_0W_0 optimization (blue, $\alpha = 32\%$). We have also included HSE06 and $HYB^{\alpha=0.17}$ ($\mu = 0.0$ Å^{-1}) from Ref. [18].

the band overlap around the Fermi level agree, but the band dispersions do as well. Dynamical effects in the self-energy seem important around −3 eV where the *pd* mixed flat band is shifted downward in the hybrid functional with respect to G_0W_0. Experiments place this band somewhere in between [79]. In Fig. 4 we have superimposed the same results on an ARPES experiment by Rohwer *et al.* [77]. Since spin-orbit coupling (SOC) is not included, care should be taken when comparing with experiment. Previous studies have shown that SOC splits the degenerate *p*-bands at Γ, which could have a small effect on the comparisons. Overall we see a very good agreement between theory and experiment noting that some of the deviations can be explained by looking at different values for k_z (see the discussion in Ref. [18]).

To the right in Fig. 5 we have compared an unoccupied *d*-orbital of the local hybrid with the same orbital of the nonlocal hybrid. The orbitals are very similar despite very different underlying gaps. The same is true for EXX_c/HF_c to the left in the figure, suggesting that not only the density but also orbitals are well-mimicked by the local KS potential. The effect of exchange on the *d*-orbitals might be one explanation for the sensitivity of G_0W_0 to the fraction of exchange in the starting-point. The larger α is, the more charge is localized between the Ti atoms. The charge on the Se atoms, i.e., the hybridization with Se-*p*-orbitals, is instead seen to reduce with α. The H-G_0W_0 yields a gap of 0.4 eV at 32% of exchange, which is much larger than any experimental value. We also performed a self-consistent COHSEX calculation, which gives a more reasonable result of 0.12 eV. We stress that these gaps are not related to the CDW since the symmetry is preserved in our calculations.

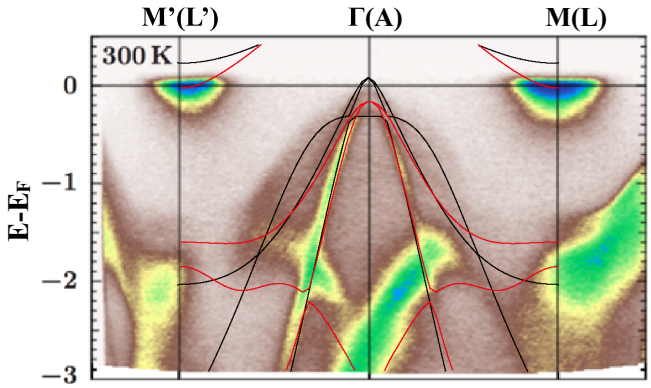

FIG. 4. Band structure of $HYB^{\alpha=0.2}$ compared to ARPES at 300 K [77]. Red lines correspond to the *A*-*L* path and black lines to the Γ-*M* path.

C. RPA optimized hybrid functional

The approach applied above shows that G_0W_0 predicts a value for the *pd* band-overlap that is in good agreement with many experiments. It also gives us a prediction for α based on the derivative of the RPA functional. This hybrid functional can now be used to study the CDW instability, too expensive for an approach like *GW* or RPA. For an in-depth analysis of the CDW instability with hybrid functionals, we

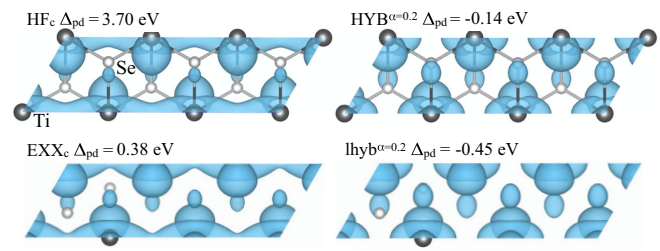

FIG. 5. Isosurface of a Ti-*d*-orbital along the Γ-*M* path [80]. To the left, EXX_c is compared to HF_c, and to the right the optimal hybrid with 20% of nonlocal exchange is compared to the corresponding local hybrid approximation.

refer the reader to Ref. [18]. Here we will restrict ourselves to a comparison between the hybrid functionals obtained via the different optimization procedures described in Sec. II.

To the right in Fig. 3 we have used the RPA optimized α to calculate the energy gain in the supercell after distorting the atoms according to the CDW pattern. We have included both HSE06 and the "best" hybrid functional ($\alpha = 0.17,\ \mu = 0.0\ \text{Å}^{-1}$) from Ref. [18] for comparison. The set of parameters $\alpha = 0.2,\ \mu = 0.1\ \text{Å}^{-1}$ lies very close to the (α, μ) path used in Ref. [18] and is not so different from the set that agreed best with experiment. Note, however, that in contrast to Ref. [18], where the α-parameter was fitted to the band gap and the phonon frequencies, here it results from a self-consistent calculation.

If we look at the results for the H-G_0W_0 optimized hybrid functional with 32% of exchange and a gap of 0.4 eV, we see that the energy gain strongly reduces. Both the energy gain and the δTi distortion worsen as compared to PBE. Given that the PBE underestimates the phonon mode associated with the CDW amplitude, we do not expect this hybrid functional to accurately capture the CDW phase.

IV. CONCLUSIONS

In this work, we have applied a self-consistent *GW* method to $TiSe_2$ in order to determine the much debated band-gap/band-overlap without adjustable parameters. We have also provided a theoretical justification for the choice of hybrid functional, i.e., the amount of admixture of exact exchange.

First of all, it was found that the standard G_0W_0 prescription based on a PBE/LDA starting-point is unreliable due to qualitative errors in describing the band structure within PBE/LDA. To overcome this problem, we have developed a simple quasi-self-consistent approach based on the local hybrid potential and the RPA functional. This approach allows for a systematic inclusion of exact-exchange in the starting-point, which, in the case of $TiSe_2$, has a large impact on, e.g., the description of the Ti-*d*-orbitals and the resulting *pd* gap. It is shown that G_0W_0 converges to a semimetallic ground state with a band overlap of 0.1 eV. This is in line with transport experiments and many ARPES results, but it contradicts the first G_0W_0 results based on the LDA starting-point.

The G_0W_0 approach generates a hybrid α-parameter consistent with RPA. With a motivated choice for μ, this hybrid functional produces an electron-phonon coupling strong enough to induce the CDW transition. Furthermore, the potential energy surface lies very close to our earlier published hybrid results, which gave very accurate phonons. While in our previous work the α-parameter was chosen as a best fit to both the band gap and the phonon frequencies, here it has been calculated via a self-consistent procedure involving the G_0W_0 method. The results are very similar, providing further support to the proposed mechanism of the CDW distortion in $TiSe_2$.

ACKNOWLEDGMENTS

This work was performed using HPC resources from GENCI-TGCC/CINES/IDRIS (Grant No. A0050907625). M.H. and L.B. acknowledge support from Emergence-Ville de Paris. L.W. and M.C. acknowledge financial support from Agence Nationale de la Recherche (Grant No. ANR-19-CE24-0028) and the Fond National de Recherche, Luxembourg via project INTER/19/ANR/13376969/ACCEPT.

[1] A. F. Kusmartseva, B. Sipos, H. Berger, L. Forró, and E. Tutiš, Pressure Induced Superconductivity in Pristine $1T - TiSe_2$, Phys. Rev. Lett. **103**, 236401 (2009).

[2] E. Morosan, H. W. Zandbergen, B. S. Dennis, J. W. G. Bos, Y. Onose, T. Klimczuk, A. P. Ramirez, N. P. Ong, and R. J. Cava, Superconductivity in Cu_xTiSe_2, Nat. Phys. **2**, 544 (2006).

[3] F. J. Di Salvo, D. E. Moncton, and J. V. Waszczak, Electronic properties and superlattice formation in the semimetal $TiSe_2$, Phys. Rev. B **14**, 4321 (1976).

[4] J. A. Holy, K. C. Woo, M. V. Klein, and F. C. Brown, Raman and infrared studies of superlattice formation in $TiSe_2$, Phys. Rev. B **16**, 3628 (1977).

[5] F. Weber, S. Rosenkranz, J.-P. Castellan, R. Osborn, G. Karapetrov, R. Hott, R. Heid, K.-P. Bohnen, and A. Alatas, Electron-Phonon Coupling and the Soft Phonon Mode in $TiSe_2$, Phys. Rev. Lett. **107**, 266401 (2011).

[6] C. S. Snow, J. F. Karpus, S. L. Cooper, T. E. Kidd, and T.-C. Chiang, Quantum Melting of the Charge-Density-Wave State in $1T - TiSe_2$, Phys. Rev. Lett. **91**, 136402 (2003).

[7] Th. Pillo, J. Hayoz, H. Berger, F. Lévy, L. Schlapbach, and P. Aebi, Photoemission of bands above the Fermi level: The excitonic insulator phase transition in $1T - TiSe_2$, Phys. Rev. B **61**, 16213 (2000).

[8] T. E. Kidd, T. Miller, M. Y. Chou, and T.-C. Chiang, Electron-Hole Coupling and the Charge Density Wave Transition in $TiSe_2$, Phys. Rev. Lett. **88**, 226402 (2002).

[9] K. Rossnagel, L. Kipp, and M. Skibowski, Charge-density-wave phase transition in $1T - TiSe_2$: Excitonic insulator versus band-type Jahn-Teller mechanism, Phys. Rev. B **65**, 235101 (2002).

[10] H. Cercellier, C. Monney, F. Clerc, C. Battaglia, L. Despont, M. G. Garnier, H. Beck, P. Aebi, L. Patthey, H. Berger, and L. Forró, Evidence for an Excitonic Insulator Phase in $1T - TiSe_2$, Phys. Rev. Lett. **99**, 146403 (2007).

[11] C. Monney, H. Cercellier, F. Clerc, C. Battaglia, E. F. Schwier, C. Didiot, M. G. Garnier, H. Beck, P. Aebi, H. Berger, L. Forró, and L. Patthey, Spontaneous exciton condensation in $1T$-$TiSe_2$: BCS-like approach, Phys. Rev. B **79**, 045116 (2009).

[12] P. Chen, Y. H. Chan, X. Y. Fang, Y. Zhang, M. Y. Chou, S. K. Mo, Z. Hussain, A. V. Fedorov, and T. C. Chiang, Charge density wave transition in single-layer titanium diselenide, Nat. Commun. **6**, 8943 (2015).

[13] M.-L. Mottas, T. Jaouen, B. Hildebrand, M. Rumo, F. Vanini, E. Razzoli, E. Giannini, C. Barreteau, D. R. Bowler, C. Monney, H. Beck, and P. Aebi, Semimetal-to-semiconductor transition and charge-density-wave suppression in $1T - TiSe_{2-x}S_x$ single crystals, Phys. Rev. B **99**, 155103 (2019).

[14] A. Kogar, M. S. Rak, S. Vig, A. A. Husain, F. Flicker, Y. Il. Joe, L. Venema, G. J. MacDougall, T. C. Chiang, E. Fradkin, J. van Wezel, and P. Abbamonte, Signatures of exciton condensation in a transition metal dichalcogenide, Science **358**, 1314 (2017).

[15] M. Calandra and F. Mauri, Charge-Density Wave and Superconducting Dome in $TiSe_2$ from Electron-Phonon Interaction, Phys. Rev. Lett. **106**, 196406 (2011).

[16] R. Bianco, M. Calandra, and F. Mauri, Electronic and vibrational properties of $TiSe_2$ in the charge-density-wave phase from first principles, Phys. Rev. B **92**, 094107 (2015).

[17] P. Chen, Y.-H. Chan, X.-Y. Fang, S.-K. Mo, Z. Hussain, A.-V. Fedorov, M.Y. Chou, and T.-C. Chiang, Hidden order and dimensional crossover of the charge density waves in $TiSe_2$, Sci. Rep. **6**, 37910 (2016).

[18] M. Hellgren, J. Baima, R. Bianco, M. Calandra, F. Mauri, and L. Wirtz, Critical Role of the Exchange Interaction for the Electronic Structure and Charge-Density-Wave Formation in $TiSe_2$, Phys. Rev. Lett. **119**, 176401 (2017).

[19] V. I. Anisimov, J. Zaanen, and O. K. Andersen, Band theory and Mott insulators: Hubbard *U* instead of stoner *I*, Phys. Rev. B **44**, 943 (1991).

[20] M. Hellgren, J. Baima, and A. Acheche, Exciton Peierls mechanism and universal many-body gaps in carbon nanotubes, Phys. Rev. B **98**, 201103(R) (2018).

[21] D. Pasquier and O. V. Yazyev, Excitonic effects in two-dimensional $TiSe_2$ from hybrid density functional theory, Phys. Rev. B **98**, 235106 (2018).

[22] L. Hedin, New method for calculating the one-particle Green's function with application to the electron-gas problem, Phys. Rev. **139**, A796 (1965).

[23] B. Holm and U. von Barth, Fully self-consistent *GW* self-energy of the electron gas, Phys. Rev. B **57**, 2108 (1998).

[24] G. Strinati, H. J. Mattausch, and W. Hanke, Dynamical Correlation Effects on the Quasiparticle Bloch States of a Covalent Crystal, Phys. Rev. Lett. **45**, 290 (1980).

[25] M. S. Hybertsen and S. G. Louie, Electron correlation in semiconductors and insulators: Band gaps and quasiparticle energies, Phys. Rev. B **34**, 5390 (1986).

[26] F. Aryasetiawan and O. Gunnarsson, The GW method, Rep. Prog. Phys. **61**, 237 (1998).

[27] L. Reining, The GW approximation: content, successes and limitations, WIREs Comput. Mol. Sci. **8**, e1344 (2017).

[28] F. Bruneval, N. Vast, and L. Reining, Effect of self-consistency on quasiparticles in solids, Phys. Rev. B **74**, 045102 (2006).

[29] M. van Schilfgaarde, T. Kotani, and S. Faleev, Quasiparticle Self-Consistent *GW* Theory, Phys. Rev. Lett. **96**, 226402 (2006).

[30] M. Shishkin and G. Kresse, Self-consistent *GW* calculations for semiconductors and insulators, Phys. Rev. B **75**, 235102 (2007).

[31] V. Atalla, M. Yoon, F. Caruso, P. Rinke, and M. Scheffler, Hybrid density functional theory meets quasiparticle calculations: A consistent electronic structure approach, Phys. Rev. B **88**, 165122 (2013).

[32] R. W. Godby, M. Schlüter, and L. J. Sham, Trends in self-energy operators and their corresponding exchange-correlation potentials, Phys. Rev. B **36**, 6497 (1987).

[33] R. W. Godby, M. Schlüter, and L. J. Sham, Self-energy operators and exchange-correlation potentials in semiconductors, Phys. Rev. B **37**, 10159 (1988).

[34] M. Grüning, A. Marini, and A. Rubio, Density functionals from many-body perturbation theory: The band gap for semiconductors and insulators, J. Chem. Phys. **124**, 154108 (2006).

[35] M. Hellgren and U. von Barth, Correlation potential in density functional theory at the GWA level: Spherical atoms, Phys. Rev. B **76**, 075107 (2007).

[36] M. Hellgren, D. R. Rohr, and E. K. U. Gross, Correlation potentials for molecular bond dissociation within the self-consistent random phase approximation, J. Chem. Phys. **136**, 034106 (2012).

[37] Y. M. Niquet and X. Gonze, Band-gap energy in the random-phase approximation to density-functional theory, Phys. Rev. B **70**, 245115 (2004).

[38] J. Klimes and G. Kresse, Kohn-Sham band gaps and potentials of solids from the optimised effective potential method within the random phase approximation, J. Chem. Phys. **140**, 054516 (2014).

[39] M. Cazzaniga, H. Cercellier, M. Holzmann, C. Monney, P. Aebi, G. Onida, and V. Olevano, Ab initio many-body effects in $TiSe_2$: A possible excitonic insulator scenario from GW band-shape renormalization, Phys. Rev. B **85**, 195111 (2012).

[40] G. Baym and L. P. Kadanoff, Conservation laws and correlation functions, Phys. Rev. **124**, 287 (1961).

[41] G. Baym, Self-consistent approximations in many-body systems, Phys. Rev. **127**, 1391 (1962).

[42] A. Klein, Perturbation theory for an infinite medium of fermions. ii, Phys. Rev. **121**, 950 (1961).

[43] G. Strinati, H. J. Mattausch, and W. Hanke, Dynamical aspects of correlation corrections in a covalent crystal, Phys. Rev. B **25**, 2867 (1982).

[44] M. E. Casida, Generalization of the optimized-effective-potential model to include electron correlation: A variational derivation of the Sham-Schlüter equation for the exact exchange-correlation potential, Phys. Rev. A **51**, 2005 (1995).

[45] F. Caruso, D. R. Rohr, M. Hellgren, X. Ren, P. Rinke, A. Rubio, and M. Scheffler, Bond Breaking and Bond Formation: How Electron Correlation is Captured in Many-Body Perturbation Theory and Density-Functional Theory, Phys. Rev. Lett. **110**, 146403 (2013).

[46] M. Hellgren, F. Caruso, D. R. Rohr, X. Ren, A. Rubio, M. Scheffler, and P. Rinke, Static correlation and electron localization in molecular dimers from the self-consistent RPA and *GW* approximation, Phys. Rev. B **91**, 165110 (2015).

[47] L. J. Sham and M. Schlüter, Density-Functional Theory of the Energy Gap, Phys. Rev. Lett. **51**, 1888 (1983).

[48] J. P. Perdew, R. G. Parr, M. Levy, and J. L. Balduz, Density-Functional Theory for Fractional Particle Number: Derivative Discontinuities of the Energy, Phys. Rev. Lett. **49**, 1691 (1982).

[49] O. Gunnarsson and K. Schönhammer, Density-Functional Treatment of an Exactly Solvable Semiconductor Model, Phys. Rev. Lett. **56**, 1968 (1986).

[50] M. Hellgren and E. K. U. Gross, Discontinuities of the exchange-correlation kernel and charge-transfer excitations in time-dependent density-functional theory, Phys. Rev. A **85**, 022514 (2012).

[51] M. Hellgren and E. K. U. Gross, Discontinuous functional for linear-response time-dependent density-functional theory: The exact-exchange kernel and approximate forms, Phys. Rev. A **88**, 052507 (2013).

[52] J. Heyd, G. E. Scuseria, and M. Ernzerhof, Hybrid functionals based on a screened coulomb potential, J. Chem. Phys. **118**, 8207 (2003).

[53] J. D. Talman and W. F. Shadwick, Optimized effective atomic central potential, Phys. Rev. A **14**, 36 (1976).
[54] M. Städele, J. A. Majewski, P. Vogl, and A. Görling, Exact Kohn-Sham Exchange Potential in Semiconductors, Phys. Rev. Lett. **79**, 2089 (1997).
[55] E. Engel and R. N. Schmid, Insulating Ground States of Transition-Metal Monoxides from Exact Exchange, Phys. Rev. Lett. **103**, 036404 (2009).
[56] M. Kuisma, J. Ojanen, J. Enkovaara, and T. T. Rantala, Kohn-Sham potential with discontinuity for band gap materials, Phys. Rev. B **82**, 115106 (2010).
[57] E. J. Baerends, From the Kohn-Sham band gap to the fundamental gap in solids. an integer electron approach, Phys. Chem. Chem. Phys. **19**, 15639 (2017).
[58] C. Mitra, Extracting the hybrid functional mixing parameter from a GW quasiparticle approach, Physica Status Solidi B **250**, 1449 (2013).
[59] S. Ismail-Beigi, Correlation energy functional within the *GW*-RPA: Exact forms, approximate forms, and challenges, Phys. Rev. B **81**, 195126 (2010).
[60] N. Schwentner, F. J. Himpsel, V. Saile, M. Skibowski, W. Steinmann, and E. E. Koch, Photoemission from Rare-Gas Solids: Electron Energy Distributions from the Valence Bands, Phys. Rev. Lett. **34**, 528 (1975).
[61] R. M. Chrenko, Ultraviolet and infrared spectra of cubic boron nitride, Solid State Commun. **14**, 511 (1974).
[62] M. Betzinger, C. Friedrich, A. Görling, and S. Blügel, Precise response functions in all-electron methods: Application to the optimized-effective-potential approach, Phys. Rev. B **85**, 245124 (2012).
[63] H. A. Al-Brithen, A. R. Smith, and D. Gall, Surface and bulk electronic structure of ScN(001) investigated by scanning tunneling microscopy/spectroscopy and optical absorption spectroscopy, Phys. Rev. B **70**, 045303 (2004).
[64] C. Wang, L. Dotson, M. McKelvy, and W. Glaunsinger, Scanning tunneling spectroscopy investigation of charge transfer in model intercalation compounds $Ti_{1+x}S_2$, J. Phys. Chem. **99**, 8216 (1995).
[65] A. Svane, N. E. Christensen, I. Gorczyca, M. van Schilfgaarde, A. N. Chantis, and T. Kotani, Quasiparticle self-consistent GW theory of iii-v nitride semiconductors: Bands, gap bowing, and effective masses, Phys. Rev. B **82**, 115102 (2010).
[66] A. Stoliaroff, S. Jobic, and C. Latouche, Optoelectronic properties of TiS_2: A never ended story tackled by density functional theory and many-body methods, Inorg. Chem. **58**, 1949 (2019).
[67] G. Kresse and J. Furthmüller, Efficient iterative schemes for ab initio total-energy calculations using a plane-wave basis set, Phys. Rev. B **54**, 11169 (1996).
[68] G. Kresse and J. Furthmüller, Efficiency of ab-initio total energy calculations for metals and semiconductors using a plane-wave basis set, Comput. Mater. Sci. **6**, 15 (1996).
[69] G. Kresse and D. Joubert, From ultrasoft pseudopotentials to the projector augmented-wave method, Phys. Rev. B **59**, 1758 (1999).
[70] P. Giannozzi *et al.*, Advanced capabilities for materials modeling with Quantum ESPRESSO, J. Phys.: Condens. Matter **29**, 465901 (2017).
[71] R. Dovesi, A. Erba, R. Orlando, C. M. Zicovich-Wilson, B. Civalleri, L. Maschio, M. Rérat, S. Casassa, J. Baima, S. Salustro, and B. Kirtman, Quantum-mechanical condensed matter simulations with crystal, WIREs Computat. Molec. Sci. **8**, e1360 (2018).
[72] N. L. Nguyen, N. Colonna, and S. de Gironcoli, Ab initio self-consistent total-energy calculations within the EXX/RPA formalism, Phys. Rev. B **90**, 045138 (2014).
[73] A. Marini, C. Hogan, M. Grüning, and D. Varsano, yambo: An *ab initio* tool for excited state calculations, Comp. Phys. Commun. **180**, 1392 (2009).
[74] D. Sangalli *et al.*, Many-body perturbation theory calculations using the yambo code, J. Phys.: Condens. Matter **31**, 325902 (2019).
[75] J. Klimes, M. Kaltak, and G. Kresse, Predictive *GW* calculations using plane waves and pseudopotentials, Phys. Rev. B **90**, 075125 (2014).
[76] T. Rangel, M. Del Ben, D. Varsano, G. Antonius, F. Bruneval, F. H. da Jornada, M. J. van Setten, O. K. Orhan, D. D. O'Regan, A. Canning, A. Ferretti, A. Marini, G.-M. Rignanese, J. Deslippe, S. G. Louie, and J. B. Neaton, Reproducibility in G_0W_0 calculations for solids, Comput. Phys. Commun. **255**, 107242 (2020).
[77] T. Rohwer, S. Hellmann, M. Wiesenmayer, C. Sohrt, A. Stange, B. Slomski, A. Carr, Y. Liu, L. M. Avila, M. Kallane, S. Mathias, L. Kipp, K. Rossnagel, and M. Bauer, Collapse of long-range charge order tracked by time-resolved photoemission at high momenta, Nature (London) **471**, 490 (2011).
[78] A. Qteish, P. Rinke, M. Scheffler, and J. Neugebauer, Exact-exchange-based quasiparticle energy calculations for the band gap, effective masses, and deformation potentials of ScN, Phys. Rev. B **74**, 245208 (2006).
[79] Z. Vydrova, E. F. Schwier, G. Monney, T. Jaouen, E. Razzoli, C. Monney, B. Hildebrand, C. Didiot, H. Berger, T. Schmitt, V. N. Strocov, F. Vanini, and P. Aebi, Three-dimensional momentum-resolved electronic structure of $1T - TiSe_2$: a combined soft-x-ray photoemission and density functional theory study, Phys. Rev. B **91**, 235129 (2015).
[80] The iso-surface of the square of the Bloch orbitals are visualized with VESTA [K. Momma and F. Izumi, VESTA 3 for three-dimensional visualization of crystal, volumetric and morphology data, J. Appl. Crystallogr., **44**, 1272 (2011)].